Bound Water in Articular Cartilage

Bachelor of Science Thesis

Katja Tolkkinen
Physics Degree Program
Faculty of Science
University of Oulu

11.11.2019

Supervisors: Ville-Veikko Telkki and Sarah Mailhiot

Contents

1 Introduction

Osteoarthritis is a disease in which articular cartilage, a softening and pressure-bearing surface on the bone, degenerates. Osteoarthritis is the most common joint disease in the world with the predominant symptoms being pain and disability. Although osteoarthritis is a widely studied disease worldwide, the mechanism of its development is still not fully understood and no curative treatment has been developed for end-stage osteoarthritis. Research on articular cartilage is important to detect the disease in early-stage and to develop new treatments [1,2].

Nuclear Magnetic Resonance (NMR) is a phenomenon which occurs when an atomic nucleus interacts with an external magnetic field. NMR spectroscopy is one of the most versatile research methods for biological research because it is non-invasive due to use of non-ionizing radio frequency radiation. NMR provides exact information on the structure and chemical environment of biomolecules without damaging a sample. In addition, one of the most important applications of NMR, magnetic resonance imaging (MRI), enables the study of biological systems from the molecular level to the scale of an entire human being [3,4].

The purpose of this thesis is to study the bound water and porous structure of articular cartilage. Bound water is water bound to microscopic pore structures and to large macromolecules and because bound water has properties that differ from bulk water, the bound and bulk water can be distinguished by NMR. The first chapters of this thesis introduce the structure of articular cartilage as well as the basic principles of NMR. Finally, there is an experimental part where is introduced the NMR cryoporometry experiments carried out with human cartilage samples and artificial gel samples modelling the composition of articular cartilage [5,6].

2 Articular cartilage

A joint is a space between two articulating surfaces and it allows bones to slide past each other (Figure 1). The surface of a bone is covered by articular cartilage which most important tasks are to withstand pressure, act as a softening surface and prevent bones from rubbing against each other. Certain risk factors, especially ageing, overweight and hereditary, may damage the articular cartilage and make it thinner. Decay of articular cartilage, also known as an osteoarthritis, is the world's most

common type of arthritis and the most dominant symptom of which is a disability causing pain [1,2,9].

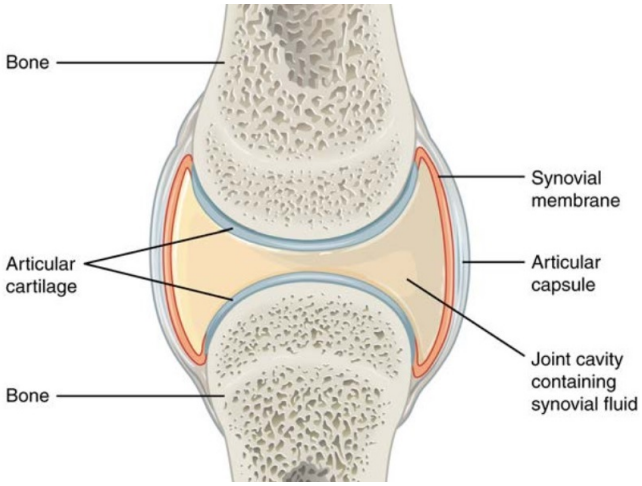

Figure 1: Structure of a synovial joint. The joint is surrounded by an articular capsule that is attached to the ends of the bones. Its inner layer, also called a synovial membrane, produces fluid that oils the joints and reduces friction between the bones. The joint is held together by the muscles attached to the bones by tendons. Ends of the bones are covered by articular cartilage which suppresses the pressure on the joint. *Anatomy and Physiology* [1].

2.1 Structure of articular cartilage

Articular cartilage is a specialized connective tissue type on the surface of the joint at the end of the bones. Articular cartilage consists of glass-like hyaline and its thickness is about 2 to 4 mm. Cartilage differs from other tissues because it does not have blood vessels, nerves or lymphatic vessels and it gets its nutrition from synovial fluid by diffusion.

The most important building blocks of articular cartilage are cartilage cells, also called chondrocytes, having approximately 10 μm diameter, and porous extracellular matrix consisting of water, collagen and proteoglycans. The cartilage consists mainly of water and because water is almost uncompressed, its main function is to withstand joint pressure. Collagen fibres give cartilage tensile and shear strength and its glassy transparent appearance. The most common collagen type in articular cartilage is collagen type II (90-95 %) which is responsible for providing tensile strength for the cartilage. Collagens I, IV, V, VI, IX and XI appear in small amounts and their task is

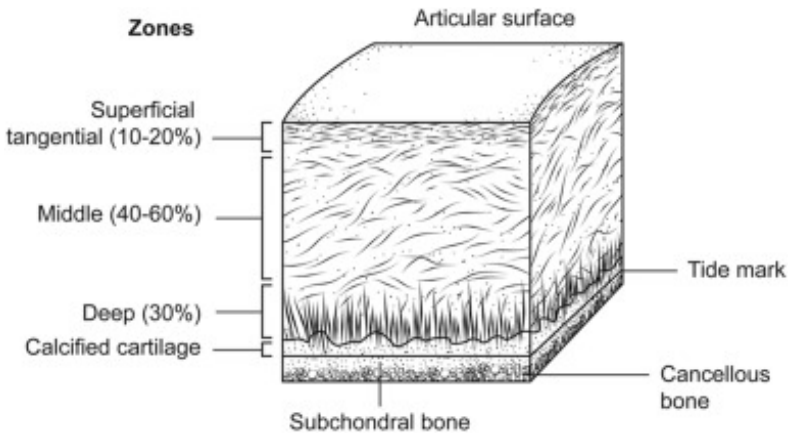

Figure 2: Structure of cartilage. From cross-sectional view, three zones of cartilage can be distinguished: the surface zone, the middle zone and the deep zone. In the surface zone, chondrocytes and collagen fibres are flattened and tightly close together in the transverse direction. In the middle zone, they are sparse and randomly spread throughout the tissue area. In the deep zone, they are parallel and form vertical columnar structures. Between cartilage and bone there is a layer of calcified cartilage that attaches the cartilage to the bone. *Brody LT, 2015* [7]. *Permission asked.*

to stabilize the fibril network of collagen type II. The structure of articular cartilage is visualized in Figure 2.

Proteoglycans provide compressive strength and the glycosaminoglycans (GAG), the subunits of proteoglycans, maintain fluid and electrolyte balance in the cartilage tissue. Because GAGs have negative charge, they attract positively charged ions, especially sodium (Na^+), which increases osmolarity in cartilage. The most common proteoglycan in cartilage tissue is large aggrecan (Figure 3) which consists of more than one hundred chondroitin and keratin sulfate chains. Chondroitin and keratin sulfates are GAGs composing of large number of alternating sugar chains that are attached to a core protein. Aggrecan is a particularly important part of cartilage because it tends to form large macromolecules with hyaluronan giving cartilage its osmotic and pressure-resistant properties. In addition to large aggrecans, there are also small amounts of proteoglycans called decorin, biglycan and fibromodulin.

The proportion of the chondrocytes in cartilage volume is about 1-5 % and their task is to synthesize the components of extracellular matrix and maintain cartilage metabolism. The extracellular matrix also contains ions, lipids, phospholipids and noncollagenous proteins [9-11].

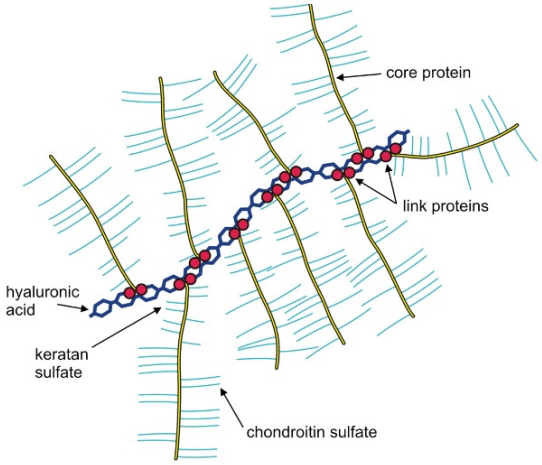

Figure 3: Aggregans bound to hyaluronan. *Oussorena E et al, 2011* [8]. *Permission asked.*

2.2 Osteoarthritis

About one million Finns suffer from osteoarthritis (OA) and due to that it is the most common joint disease in Finland. The development of OA takes years and its most prominent symptoms in the end-stage of the disease are joint pain, stiffness and dysfunction. Most commonly, OA occurs in knees, hips and fingers.

The intristic cause of OA is a little innate ability of chondrocytes for regeneration in the case of aging and injury. Chondrocytes maintain and rebuild homeostatic conditions of cartilage by synthesizing components of the extracellular matrix. In particular, aging, sudden heavy impact or continuous load caused by obesity or physical work can damage chondrocytes. The cell division of chondrocytes is low and if chondrocytes are damaged, they are not able to repair their own cell populations. As a result, when the cells age the cell population reduces. In addition to aging and injury, heredity and some hormonal and metabolic diseases can increase the risk of OA.

As the number of chondrocytes gets lower, the amount of cartilage tissue decreases. In the early stages of OA, the surface of the cartilage begins to degrade. Over time, the amount of proteoglycans and collagen fibres decreases and the chondrocytes begin to form clusters. Also, the proteoglycans exist in a nonaggregated form, unbound to hyaluron and the chain length of the proteoglycan gets shorter. In OA, the subchondral bone gets thicker and the lining between the deep and calcified zones (tidemark) duplicates and there can occur vascular invasion from the subchondral bone. Ulti-

mately, the degration overcomes the regeneration which narrows the joint and makes bones to rub against each other. The primary goal of treating OA is always analgesics, exercise, losing weight and avoiding physical work. In cases of OA causing serious disability, the joint may be surgically replaced by joint implant [12-15].

2.3 Bound water in articular cartilage

The articular cartilage mainly consist of water. In cartilage tissue, water can be either free or bound. Free or bulk water moves through the tissues by diffusion and its interaction with other molecules is based on random movement. Instead, bound water covers the microscopic pores and cavities of cartilage tissue by forming very thin organized water layers on their surface. Water molecules are electrically polarized which means that on the other side they have positive charge and the other side negative charge and, as a result, they form bonds with each other and with other electrically charged molecules. In articular cartilage, the bound water is filling the pores formed by macromolecules of the extracellular matrix. The bound water is attached especially to collagen and proteoglycans [5,6,16,17].

3 Nuclear Magnetic Resonance (NMR)

Nuclear magnetic resonance (NMR) is a phenomenon which occurs when an atomic nucleus interacts with an external magnetic field. Resonance is a phenomenon of physics in which an external force transfers energy to the system at a specific resonant frequency of this system. Resonance can be caused by an another object or, in NMR phenomenon, an oscillating magnetic field. This chapter introduces the basic principles of the NMR and this chapter is based on references [3,4,18].

3.1 Nucleus in an external magnetic field

Being familiar with the basic principles and equations of quantum mechanics is essential for understanding the NMR phenomenon. This chapter introduces how the nucleus of an atom behaves and what properties it has when it is placed in an external magnetic field.

3.1.1 Magnetic properties of a nucleus

The nucleus of an atom consists of positively charged protons and electrically neutral neutrons and it is surrounded by negatively charged electron cloud. Not all nuclei experience the NMR phenomenon because the phenomenon requires a nuclei that has a property called spin.

Spin is a feature of a particle that can be thought as a form of an internal angular momentum. The spin of a proton or a neutron has a value $\frac{1}{2}$ and it can be orientated in two ways; either spin-up or spin-down. Protons and neutrons that possess spins having opposite signs can pair up and eliminate each other. The overall spin of a nucleus can have values 0, $\frac{1}{2}$, 1, $\frac{3}{2}$ etc. and only nuclei having a nonzero net spin are significant in the NMR phenomenon.

If a nucleus has spin, it also has an intrinsic spin angular momentum $\boldsymbol{J}$. Classically, it can be thought that the nucleus having spin is actually rotating like a spinning top but, in reality, spin is a quantum mechanical quantity and the rotation is only its classic analog. Quantization is a phenomenon where, instead of a continuous distribution, a physical quantity can only get certain discrete values. The magnitude of a spin angular momentum can be defined as

$$J = |\boldsymbol{J}| = \hbar\sqrt{I(I+1)} \tag{1}$$

where $\hbar$ is reduced Planck's constant ($\hbar = \frac{h}{2\pi}$) and I is a spin quantum number of a nucleus which can have values $I = 0, \frac{1}{2}, 1, \frac{3}{2}, \ldots$

If a nucleus has a spin angular momentum, it also has a parallel magnetic dipole moment

$$\boldsymbol{\mu} = \gamma \boldsymbol{J} \tag{2}$$

where γ is a nucleus-specific gyromagnetic ratio. Because of the quantization of the spin angular momentum, the dipole moment is also quantized and its magnitude is

$$\mu = |\boldsymbol{\mu}| = \gamma\hbar\sqrt{I(I+1)}. \tag{3}$$

When a nucleus having a magnetic dipole is placed in an external magnetic field $\boldsymbol{B}$, the field produces a torque $\boldsymbol{\tau} = \boldsymbol{\mu} \times \boldsymbol{B}$ and the axis of the nucleus begins to rotate. The phenomenon is called precession, also known as a gyration movement. The spinning

frequency is called Larmor frequency and it can be defined as

$$\nu = \frac{\gamma}{2\pi} B. \tag{4}$$

3.1.2 Energy levels of a nucleus

When a magnetic dipole moment of a nucleus and the external magnetic field interact with each other, it causes a division of energy levels of a nucleus into several parts and the phenomenon is called Zeeman effect (Figure 4). The number of Zeeman states is $2I + 1$. Possible values of the energy levels can be obtained from equation

$$E = -\gamma \hbar B m \tag{5}$$

where m can have values $m = (I, I-1, I-2, ..., -I)$. Thus, the values of energy levels are also quantized. A nucleus can move from energy level to another by absorbing or emitting a photon of electromagnetic radiation. The energy of a photon depends only on the frequency of the radiation. To be able to move between two energy levels, energy of a photon must be exactly equal to the difference between the energies of two levels. When a nucleus having spin $\frac{1}{2}$ moves to next energy level ($\Delta m = \pm 1$), the energy change is $\Delta E = \pm \gamma \hbar B$ and the transition emits or absorbs a photon which frequency is

$$\nu = \frac{\Delta E}{h} = \frac{\gamma \hbar}{h} B = \frac{\gamma}{2\pi} B. \tag{6}$$

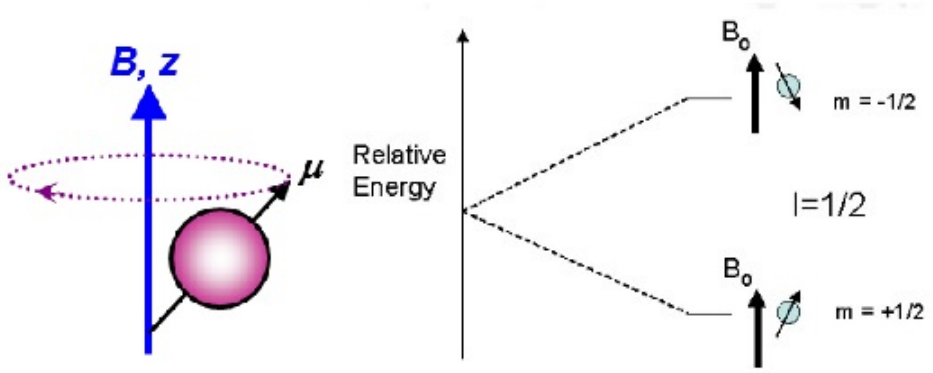

Figure 4: In an external magnetic field, the energy levels of the precessing nucleus are divided by the Zeeman effect. On left: *Telkki V, Lecture material of Spectroscopic methods* [3].*Permission asked.* On right: *Process NMR* [19].

This equation shows that the frequency of radiation required for excitation of the nucleus is equal to the Larmor's precession frequency of the nucleus.

3.1.3 The bulk magnetization

Nuclei in an external magnetic field behave as small bar magnets tending to turn to the direction of the field because then their energy is at their lowest. For example, if there is a nucleus having a spin $\frac{1}{2}$, according to Equation (5), the energy of the spin-up nucleus is lower than the spin-down nucleus due to the minus sign of the equation. Hence, most of the nuclei are orientated to spin-up state but also part of the nuclei are in spin-down state due to thermal energy. Actually, the effect of the heat movement is so significant that the difference of spin-up and spin-down states is very small and the final signal is produced by a millionth of the nuclei. Assuming that the nuclei are identical and summing up the magnetic dipole moments of all the nuclei, the magnitude of the bulk magnetization $\boldsymbol{M_0}$ parallel to external magnetic field $\boldsymbol{B_0}$ can be defined as

$$M_0 = \frac{N\gamma^2\hbar^2 I(I+1)}{3kT} B_0 \tag{7}$$

where N is the number of nuclei, k Boltzmann's constant ($k = 1.380649 \cdot 10^{-23}\ \frac{J}{K}$) and T temperature in Kelvin. The term kT describes the effect of thermal energy in a sample.

3.2 Detection of the NMR signal

Detection of the NMR phenomenon is based on a detection of the bulk magnetization in a sample. The more intense the magnetization, the stronger the signal, and it can

Nucleus	**Net spin**	**Natural abundance (%)**	**γ (MHz/T)**
^{1}H	1/2	99.98	48.58
^{2}H	1	0.02	6.54
^{13}C	1/2	1.11	10.71
^{14}N	1	99.64	3.08
^{19}F	1/2	100	40.08
^{23}Na	3/2	100	11.27
^{31}P	1/2	100	17.25

Table 1: Charasteristics of nuclei commonly used in NMR [3,18,20].

clearly be seen from Equation (7) that the signal can be increased by adding more nuclei to the sample or increasing the strength of an external magnetic field. On the contrary, raising the temperature increases the heat transfer between the atoms, randomizes spin orientation and thus weakens the signal. The gyromagnetic ratio is a specific constant for each nucleus of different atoms. The strength of the NMR signal is directly proportional to the magnitude of the gyromagnetic ratio so it is advisable to select a nucleus having a great gyromagnetic ratio. Hydrogen ^{1}H is an element which nucleus consists of only a single proton and it has the highest gyromagnetic ratio of all the isotopes of different elements. Also, the natural abundance of hydrogen is very high and for that reason it is the most used nucleus in NMR spectroscopy. Table 1 above shows some properties of nuclei commonly used in NMR.

3.2.1 RF excitation pulse

Suppose, there is a coordinate system having directions x, y and z. The sample is placed to the origin and the external magnetic field $\boldsymbol{B_0}$ is parallel to z-axis and, as a result, the magnetization vector $\boldsymbol{M}$ also points to the positive z-direction. Also, there is an excitation field $\boldsymbol{B_1}$ perpendicular to the z-axis and it is rotating about the z-axis in a transverse plane at a frequency equal to Larmor frequency. As a result, the magnetization vector $\boldsymbol{M}$ rotates to an angle θ from its equilibrium and begins to precess. A radio frequency excitation field $\boldsymbol{B_1}$ or RF-pulse is generated by placing a coil with an oscillating alternating current at the resonant frequency beside or around the sample. The length of the excitation pulse can be selected, for example, in such way that at the end of the pulse the magnetization vector forms 90^o or 180^o angle with the positive z-axis. After the pulse, the magnetization vector precesses around the z-axis and therefore the coil experiences a changing magnetic field which induces voltage to the coil. Induced voltage is directly proportional to the magnitude of the transverse component of the magnetization vector. After a certain time, the magnetization vector returns to its equilibrium to the z-axis and the radio frequency signal arriving to the coil decreases and because of that the signal is called a free induction decay signal, i.e. a FID signal.

3.3 Relaxation

When a nucleus is excited by an RF-pulse, it precesses for a while and eventually returns to its equilibrium to the z-axis. Relaxation is defined as a recovery of the magnetization vector back to its equilibrium and relaxation time describes how long the

vector takes to relax. The relaxation can be divided into longitudinal and transverse relaxation (Figure 5). Determining these relaxation times gives important information on the movement and surroundings of studied nuclei.

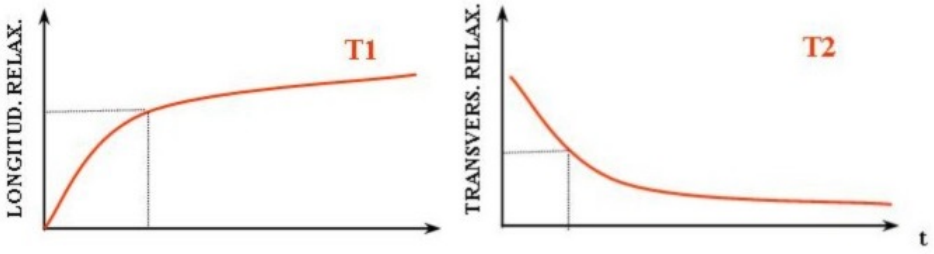

Figure 5: In relaxation, the magnitude of longitudinal component of magnetization increases and the transverse decreases. *Wikimedia Commons* [21].

3.3.1 T_1 relaxation

At equilibrium, magnetization $\boldsymbol{M}$ has only a z-direction component M_z and when it is excited its transverse component M_{xy} increases and M_z decreases accordingly. The T_1 relaxation represents the recovery of the longitudinal magnetization back to its maximum M_0 (Figure 5). On the other hand, T_1 relaxation also describes how the energy absorbed from the RF-pulse is released back to the environment. Formerly, NMR was commonly used to study lattices of solid materials and, for historical reasons, T_1 relaxation is also called spin-lattice relaxation. If magnetization is rotated to the xy-plane, the magnitude of the longitudinal magnetization component M_z after time t is

$$M_z(t) = M_0[1 - e^{-\frac{t}{T_1}}]. \tag{8}$$

One method by which the longitudinal T_1 relaxation time can be deduced is an inversion recovery experiment. At the beginning of the experiment, the magnetization is at its equilibrium along the positive z-axis. The magnetization is rotated by 180° pulse to the negative z-axis and then it is given to recover back to its equilibrium for a delay τ. In an NMR experiment, only the transverse magnetization can be detected and due to that the magnetization is now rotated by 90° pulse to xy-plane and the FID signal is observed.

3.3.2 T_2 relaxation

T_2 relaxation describes the attenuation of the transverse magnetization M_{xy} to its equilibrium value zero. T_2 relaxation time is always shorter or equal to T_1 relaxation time, in other words, the transverse magnetization decays faster than longitudinal magnetization recovers. T_2 relaxation is also, for historical reasons, called as spin-spin relaxation. If magnetization is first rotated into the transverse plane, after the time t the magnitude of the transverse magnetization is

$$M_{xy}(t) = M_0 e^{-\frac{t}{T_2}}. \tag{9}$$

T_2 relaxation occurs due to nuclei interacting with each other by rotating and creating small varying magnetic fields around each other and for that reason the magnetic field experienced by the nuclei is not completely homogeneous. Because of those small inhomogeneities, magnetization vectors flipped into the transverse plane precess with slightly different speeds in different parts of the sample and, consequently, magnetization vectors are scattering like a fan opening. This dephasing of the vectors causes T_2 relaxation.

Because the NMR signal is obtained by measuring transverse magnetization, it would be easy to deduce the T_2 relaxation time directly from the FID signal. However, the static $\boldsymbol{B_0}$ magnetic field experienced by the nucleus is usually not completely homogeneous and because of that the transverse magnetization decays more rapidly than T_2 relaxation time provides. The decay caused by these external field inhomogeneities

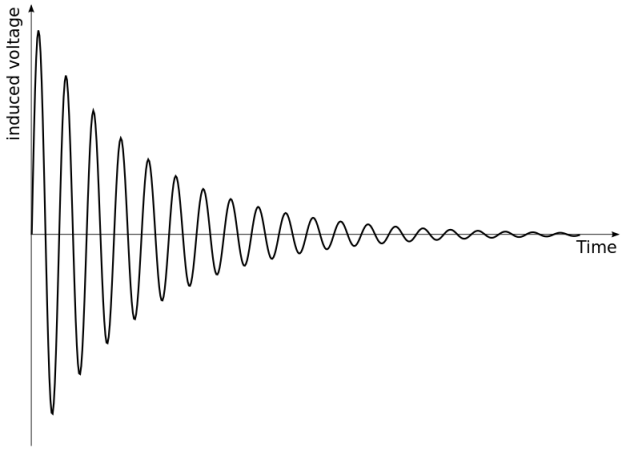

Figure 6: FID signal. *Wikimedia Commons* [22].

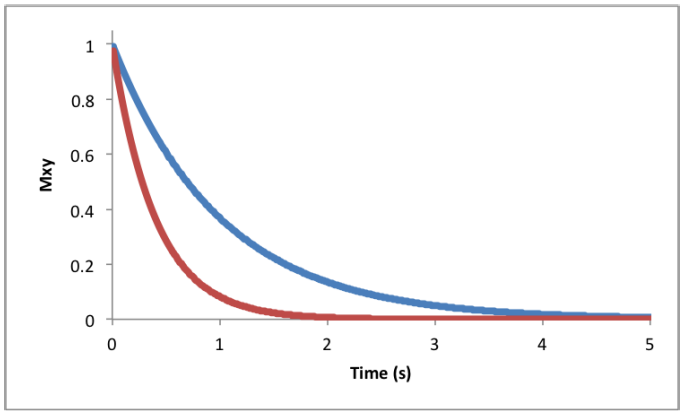

Figure 7: The blue line represents T_2 relaxation and the red line T_2^* relaxation. *Chemistry LibreTexts* [23].

can be described with relaxation time T_2^* (Figure 7).

T_2 relaxation time can be deduced with a commonly used method called spin echo pulse sequence (Figure 8). At the beginning of the experiment, the magnetization vector is at its equilibrium on the positive z-axis and after that it is rotated to the negative y-axis by a 90° pulse. Due to dephasing, transverse magnetization vectors are moving away from the y-axis and, as a result, the magnitude of the detectable magnetization decays. After the delay τ, the magnetization is flipped to the positive y-axis by a 180° pulse as a result of which the magnetization vectors are now approaching each other and they reunite at the positive y-axis. In this way, an echo can be detected and the missing signal is recovered.

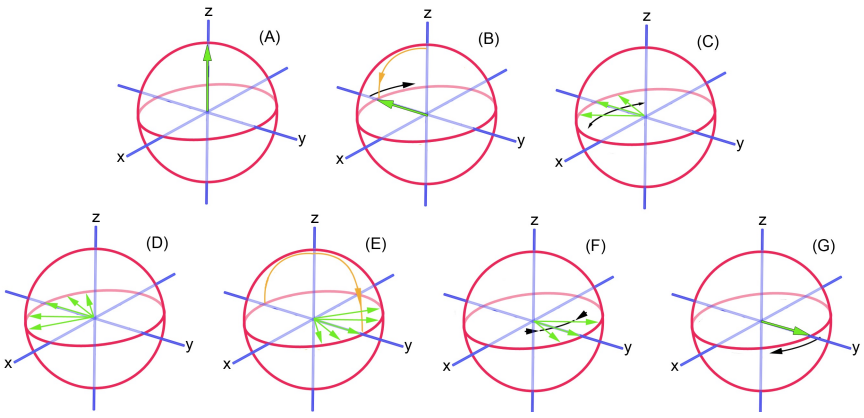

Figure 8: Spin echo pulse sequence. *Wikimedia Commons* [24].

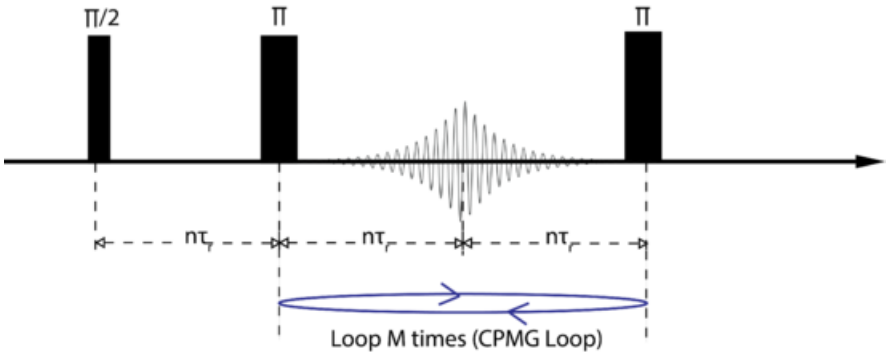

Figure 9: CPMG pulse sequence. *Chemistry LibreTexts* [25].

T_2 relaxation time can also be measured with a Carr-Purcell-Meiboom-Gill (CPMG) method which is like a spin echo pulse sequence but, instead of a single 180^o pulse, there is a series of 180^o pulses after the 90^o excitation pulse. As the 180^o pulse is repeated, the heights of the resulting echoes decay and the decay corresponds to T_2 relaxation (Figure 9).

3.4 NMR spectrum

A nucleus of an atom, usually a hydrogen nucleus or a proton, contributes an NMR signal while precessing in an external magnetic field. When all identical hydrogen nuclei experience an equally strong magnetic field, they precess at an equally high angular velocity and consequently transmit the same-frequency signal. Thus, only one single peak should be detected in an NMR spectrum. However, the magnetic field experienced by the nuclei in the sample is not constant. Instead, the electron cloud and the nearby nuclei change the magnetic field experienced by nuclei and thus different frequencies are detected. Variations of the magnetic field are only millionths of a magnitude of an external magnetic field but an exact NMR spectrometer equipment can detect easily even small frequency shifts. Thus, the NMR spectrum provides important information on molecular structures, binding angles and the chemical environment of the nuclei.

3.4.1 Chemical shift

When an atom is in an external magnetic field, its electrons circulate about the direction of the field. This electron circulation movement generates an electric current

which forms furthermore its own magnetic field which reduces a magnetic field experienced by the nucleus. The magnetic field experienced by the nucleus decreases in relation to the nucleus-specific shielding constant σ and the actual precession frequency of a nucleus is

$$\nu = \frac{\gamma}{2\pi}(1-\sigma)B_0. \tag{10}$$

The electron density varies in different parts of a molecule resulting different chemical environments. The nuclei located in different parts of the molecule precess at slightly different frequencies and the difference is called a chemical shift. From the equation above, it can be noted that the stronger the external magnetic field B_0 the greater the frequency difference and the chemical shift. This causes a problem when comparing spectra of NMR spectrometers operating at different magnetic field strengths. Therefore, chemical shift is measured in relation to a specific reference frequency ν_{ref} and it is given in parts per million (ppm). The chemical shift can be defined by an equation

$$\delta = \frac{\nu - \nu_{ref}}{\nu_{ref}} \times 10^6. \tag{11}$$

The equation shows that both the numerator and the denominator are directly proportional to the magnetic field strenght and thus the ppm values are independent of used magnetic field. Because the shielding reduces when the chemical shift increases, in the NMR spectrum the ppm values increase from right to left (Figure 10). The reference frequency ν_{ref} (0.0 ppm) is usually the operating frequency of the NMR spectrometer or the resonant frequency of tetramethylsilane (TMS). Tetramethylsilane is a commonly used reference substance in hydrogen and carbon NMR spectroscopy because it has 12 equivalent protons, i.e. they have the same a chemical environment, so it makes one clear peak to the NMR spectrum, it does not react with other substances and it can also be easily evaporated from the sample [26].

3.4.2 Interaction mechanisms between nuclei

In addition to the shielding effect described above, the magnetic field experienced by the spin-$\frac{1}{2}$-nucleus is also affected by dipole interaction and spin-spin interaction.

The adjacent nuclei can change the surrounding magnetic fields of each other through dipole interactions. Suppose there are interacting nuclei called A and B. If both nuclei are static and nucleus A is in spin-up state, now the magnetic field formed by nucleus A at the nucleus B has the same magnitude and direction but opposite sign compared to situation where A is in spin-down state. Hence, there is a dipole coupling resulting

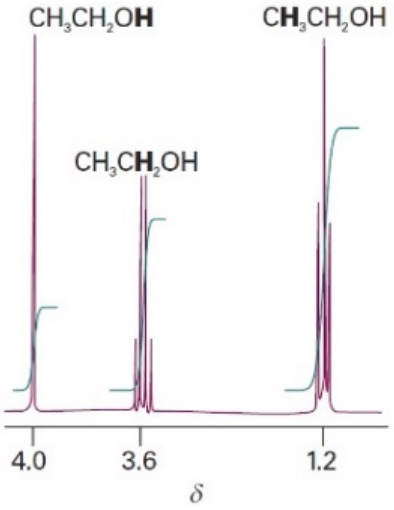

Figure 10: An NMR spectrum of ethanol. Ethanol CH_3CH_2OH has protons in three different groups and for that reason they have slightly different chemical environments and several peaks are detected in the spectrum. Protons of CH_3 and CH_2 groups locate in different parts of the molecule and consequently there is approximately 2 ppm chemical shift between them. The chemical shift of OH group is the greatest, around 4 ppm, since electronegative oxygen strongly attracts electrons of hydrogen which reduces shielding of protons and thus increases chemical shift. *Telkki V, Lecture material of Spectroscopic methods* [3]. *Permission asked.*

a distribution of the resonance frequency of the nucleus B into two spectral peaks. The distance of the peaks of the dipole coupling depends on the distance between the nuclei and their orientation in an external magnetic field. Therefore, information of the spectrum of dipole coupling can give information about molecular structures, for example, bond distances and angles. Due to isotropic rotation of molecules, dipole coupling is not detected in liquids and gases.

The interaction by which nuclei change the magnetic field of the adjacent nuclei by shared electrons is called spin-spin coupling or J coupling. If there are two coupled spin-$\frac{1}{2}$-nuclei, due to spin-spin coupling, the peaks of the spectrum are divided into two peaks corresponding to spin-up and down states of the adjacent nucleus. If there are many coupled nuclei, the spectral peaks of the coupled system are divided into several peaks and the frequency difference between the peaks is called coupling constant or the spin-spin splitting constant J. For the coupling to be observable, the coupled nuclei typically cannot locate no more than three bond lengths away from each other.

Let's look at a proton with possible spin states of $+\frac{1}{2}$ or α and $-\frac{1}{2}$ or β. Suppose that the nucleus A is coupled with two equivalent nuclei B, i.e. this is called the AB_2 spin system. Two hydrogen nuclei B have four different spin configurations that are $\alpha\alpha$, $\alpha\beta$, $\beta\alpha$ ja $\beta\beta$. The configuration $\beta\beta$ has the highest energy, $\alpha\alpha$ has the lowest energy and the energies of $\alpha\beta$ and $\beta\alpha$ are equal. Now the nucleus A can experience three different magnitudes of magnetic field caused by the nuclei B. Nuclei B can experience two different magnitudes of the magnetic field caused by nucleus A because the nucleus A can be either at α or β state. So now the resonance frequency of the nucleus A is divided into three peaks (triplet) with chemical shift δ_A and peak ratios are 1:2:1 because two spin configurations have the same energy. The resonance of the nuclei B is divided into two equally high peaks (duplet) distance of which is chemical shift δ_B.

The resonance of the nucleus A of a AB_3 spin system is divided into four spectral peaks (quartet), with a peak ratio 1:3:3:1. The coupling of AB_n spin system divides the resonance of the coupled nucleus A into $n+1$ peaks and the peak ratios follow Pascal's triangle. Unlike dipole coupling, spin-spin coupling is also observed in liquids and gases.

3.4.3 Fourier transform

In an NMR experiment, the FID signal represents the oscillation and attenuation of magnetization as a function of time. This FID signal does not give as much information as the frequency distribution signal and therefore it is advisable to transform the received signal from time to frequency domains (Figure 11).

Let's return back to the situation where the magnetization vector of a nucleus rotates at the transverse xy-plane. First, suppose that the magnetization vector is on a positive x-axis and it rotates clockwise on xy-plane. The x-component M_x gets its maximum value on the positive x-axis so by measuring the M_x it results a cosine function. Similarly, the y-component M_y gets its maximum on the positive y-axis so the signal is a sine function. The Fourier transform is a mathematical method which task is to deal with two orthogonal functions one of which is real and second imaginary. The principle of the Fourier transform is signal to be decomposed into a sum of sine and cosine waves of different frequencies and amplitudes. In this case, it can be thought that the real part of the function is the cosine function and the imaginary part is the sine function. Now, the signal of each spin group i resonating

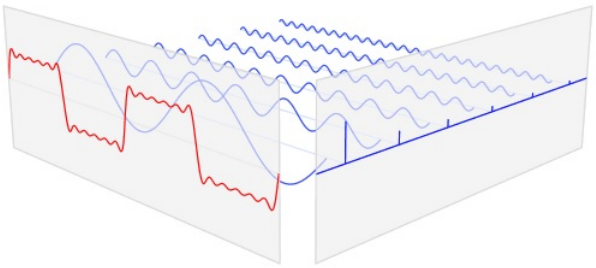

Figure 11: In the Fourier transform, the time-domain signal is converted to the frequency-domain spectrum. *Wikimedia Commons* [27].

at different frequencies ν_i after time t can be shown with x and y-components of the magnetization by equation

$$s_i = s_x^i + is_y^i = Ae^{-\frac{t}{T_2}}[\cos(2\pi\nu_i t) - i\sin(2\pi\nu_i t)] \tag{12}$$

where the term A is the amplitude of the signal. The exponent of the function describes the exponential decay of the T_2 relaxation. With the Euler's formula, the equation can be simplified to form

$$s_i = Ae^{-\frac{t}{T_2}}e^{-i2\pi\nu_i t}. \tag{13}$$

The Fourier transform of the pulse $P(t)$ can be defined as an integral

$$F(\nu) = \int_{-\infty}^{\infty} P(t)e^{-i2\pi\nu t}dt. \tag{14}$$

The Fourier transform of the signal s_i is

$$F(\nu) = \int_{0}^{\infty} s_i e^{-i2\pi\nu t}dt \tag{15}$$

and the frequency distribution is obtained by choosing only the real part of the result function

$$S(\nu) = Re\{F(s_i)\} = \frac{AT_2}{1 + 4\pi^2 T_2^2(\nu - \nu_i)}. \tag{16}$$

The equation gives a Lorenzian shape spectral peak of spins resonating at a specific frequency ν_i and the final NMR spectrum is obtained by summing up the peaks corresponding to each spin group.

3.5 NMR cryoporometry

Nuclear Magnetic Resonance Cryoporometry or NMRC is a method used in NMR spectroscopy to obtain information on the porous structure of the sample. The method is suitable for measuring pore diameters in the range 2 nm - 1 μm. NMRC is based on the Gibbs-Thomson effect whereby the freezing-melting point of liquid bound to a porous material decreases when the pore size decreases. For example, the melting point of free water is 0°C but the water bound to microscopic pores or large macromolecules melts at a noticeable lower temperature. The Gibbs-Thomson equation defines the difference between the melting points of the bound and free liquid in a spherical shaped pore as

$$\Delta T_m = T^0 - T_m = \frac{4\sigma_{sl}T^0}{H_f \rho_f x} = \frac{k}{x} \tag{17}$$

where T^0 is the melting point of the bulk liquid, T_m melting point of the liquid bound to a pore, σ_{sl} solid-liquid interface energy, H_f bulk enthalpy of fusion, ρ_f density of solid and x a diameter of a pore. Constant k is a characteristic value for studied substance.

In the ^{1}H NMRC experiment, the porous sample is placed in an NMR spectrometer and cooled until all liquid in it is frozen. After that, the sample is warmed slowly step by step and during the melting the NMR signal of the melted water is measured. Because the T_2 relaxation time of frozen water is considerably shorter than the T_2 of liquid water, freezing the sample below 0°C reduces the signal of bulk water. The signal of frozen water can be removed completely by adding a delay after the excitation pulse. If the delay is longer than the T_2 of ice, the signal of ice gets time to decay and the signal of ice can be eliminated.

When the whole sample, including the bound water, is frozen, the sample does not send any signal. The sample is then slowly melted and during that the NMR signal emitted by the sample is directly proportional to the amount of melted water and thus information on the pore size distribution, porosity, structure and amount of bound water in the sample can be deduced [28,29].

4 Experimental part

The goal of these experiments was to study bound water attached to pores and macromolecules of articular cartilage. The experiments were performed using human

articular cartilage samples and artificial protein gel samples modelling the composition of cartilage. The bound water has properties that differ from bulk water and thus the bound and bulk water can be distinguished by using the NMR cryoporometry. By using the cryoporometry, the pore size distributions, water bound to macromolecules and the T_2 relaxation times were studied.

4.1 Samples

The experiments were carried out using two types of samples: human articular cartilage samples and artificial gel samples acting as a model of cartilage.

Four cartilage samples were obtained from hips of arthritic patients at the joint surgery. However, samples containing relatively healthy cartilage were selected from the removed articular cartilage. The cartilage samples were cylindrical in shape and, in addition to cartilage tissue, they had also some bone tissue attached. One of the samples had noticeable more bone tissue attached than others (Figure 12). The samples were stored in -20°C freezer before the experiments. To moisturise and keep the pH of the samples constant, the samples were hydrated in phosphate-buffered saline (PBS).

Gel samples acted as a very simplified model of extracellular matrix of articular cartilage. The gel samples consisted of water and different collagen type I and chondroitin sulfate (CS) concentrations. The samples were made of collagen type I and CS because the goal of the experiments was to measure water bound to the protein binding sites instead of pores and for that reason it was reasonable to use protein models which have the same binding sites but different macro-pore structures. In total, there were 12 samples with collagen concentrations of 10-40 $\frac{\text{mg}}{\text{g}}$ and CS concentrations 0-20 $\frac{\text{mg}}{\text{g}}$. The gel samples were stored in -20°C freezer. The purpose of these experiments was to study the effect of change of collagen and CS concentrations on the properties

CS (mg/g) →	**0**	**5**	**10**	**20**
Collagen (mg/g)↓				
40	x	x	x	x
20			x	
10			x	

Table 2: The studied gel samples are marked with a cross.

of the samples and thus it was not necessary to measure all samples. The studied samples are marked to Table 2 above.

Figure 12: One of the four cartilage samples had noticeable more bone tissue than others. Bone (yellow) and cartilage (white) can be easily distinguished.

4.2 Experiments

Both cartilage and gel samples were inserted to 5 mm NMR tubes (Figure 13). The cartilage samples were added to tubes without extra PBS. One of the cartilage samples was previously frozen at 248 K (−25°C) with extra PBS because the first attempt was to see if the signal of extra PBS is too dominant and if all the water is frozen. ^{1}H NMR cryoporometry experiments were carried out on a Bruker Avance III 500 spectrometer using the 10-mm BBO probe (Figure 14). Freezing of the samples was performed with a liquid nitrogen evaporator.

The NMR signal of liquid water was measured using a spin echo pulse sequence with an echo time of 50 μs and CPMG pulse sequence with an echo time of 500 μs and 1000 echoes. The number of scans (NS) was 4 for cartilage samples and 8 for gel samples. The recovery delay was 10 seconds. The samples were cooled to 180 K (−93°C) and then heated back to room temperature 280 K (7°C) by 1.8 K steps. The settling delay in the experiments was 5 $\frac{\text{min}}{\text{K}}$ for spin echo, 10 $\frac{\text{min}}{\text{K}}$ for CPMG and 5

$\frac{\text{min}}{\text{scan}}$ with 0.1 K accuracy.

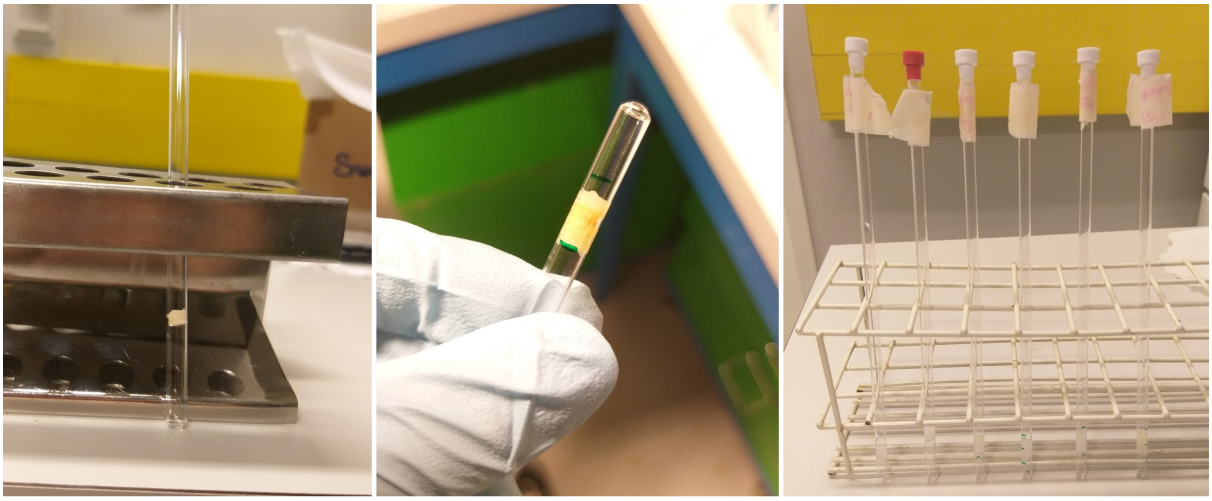

Figure 13: The samples were inserted to 5 mm NMR tubes. On left and middle, there are two cartilage samples and, on right, there are the studied gel samples.

Figure 14: The experiments were performed using a Bruker Avance III 500 spectrometer.

4.3 Results

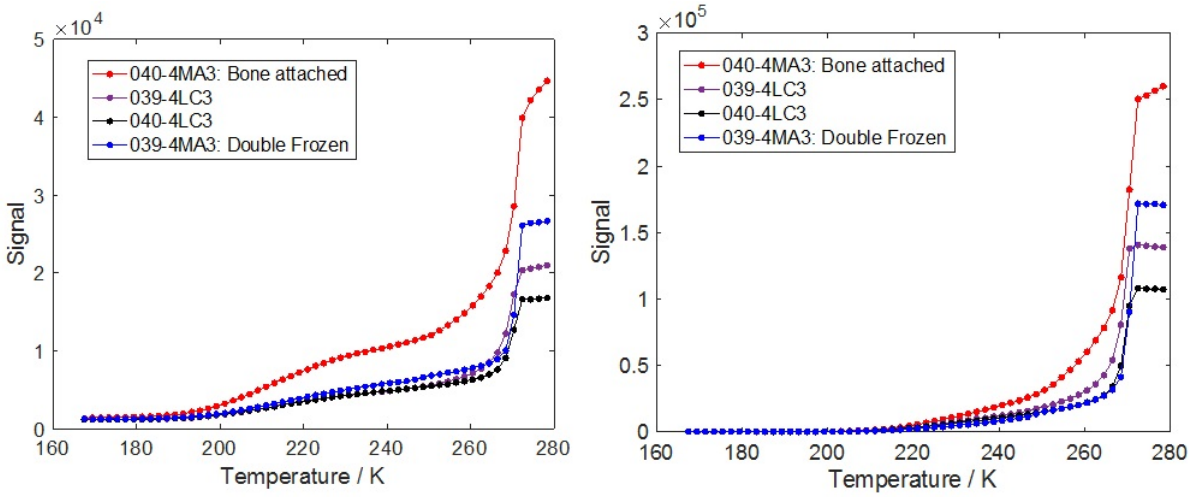

Figure 15: Comparison of 4 human cartilage samples. On left, there is spin echo data and, on right, CPMG data.

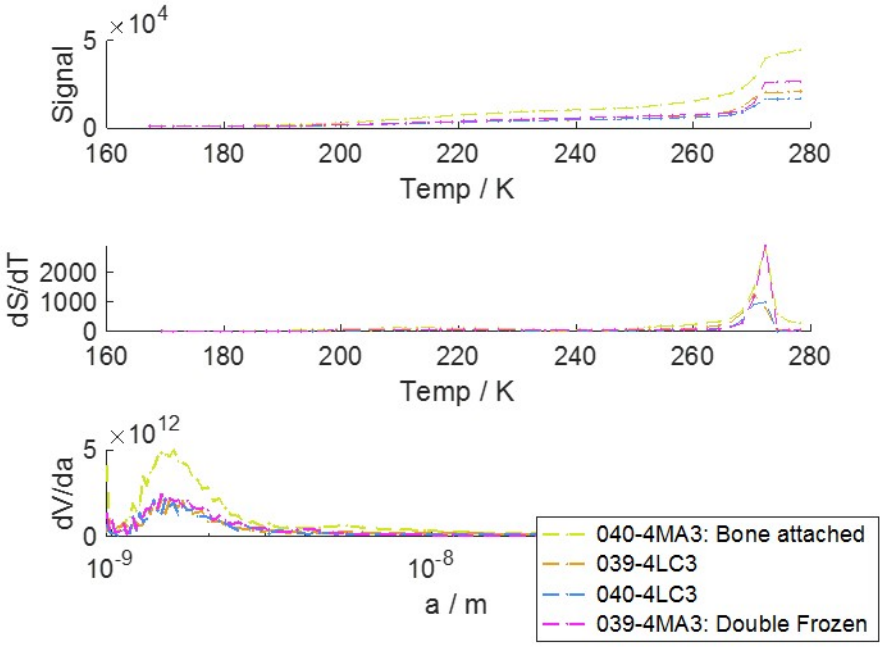

Figure 16: Spin echo data of human cartilage samples.

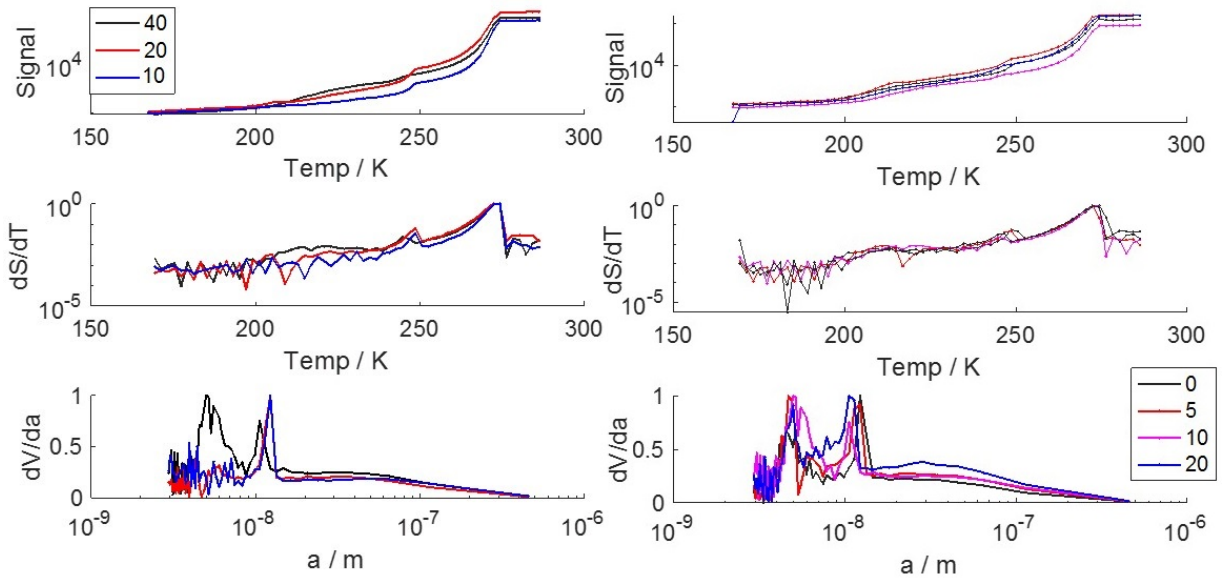

Figure 17: On left, the effect of collagen concentration and, on right, the effect of chondroitin sulfate concentration on protein gels.

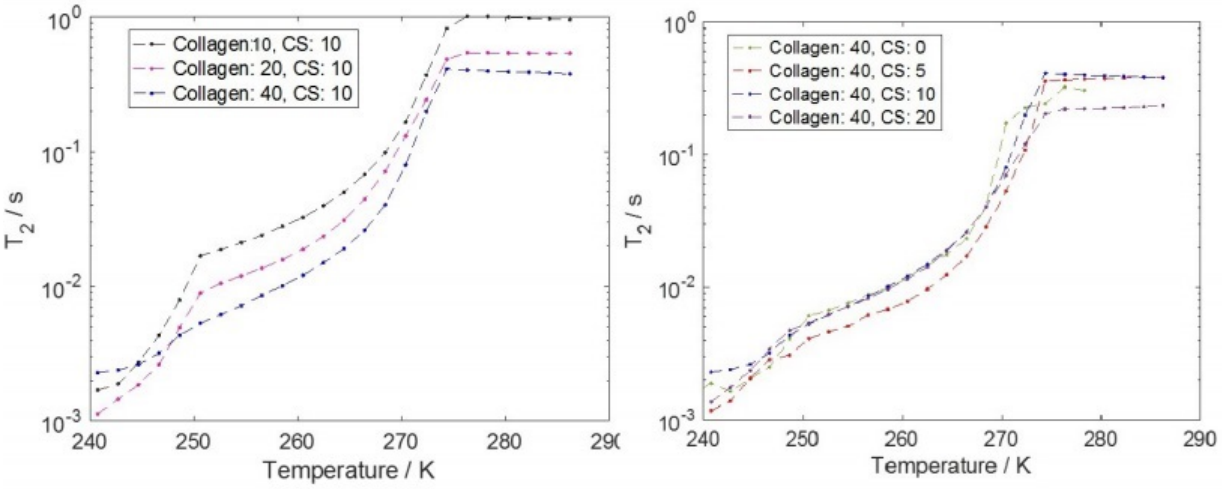

Figure 18: Effect of chondroitin sulfate and collagen on T_2 relaxation times of protein gels.

4.4 Conclusions

On Figure 15, there is a characteristic melting curve of water in microporous material. The graph on left shows spin echo data and graph on right CPMG data of the human cartilage experiments. Graphs show that when the samples are cooled to 180 K temperature, the signal is almost zero, in other words, almost all the water in samples is completely frozen. When the temperature rises, the signal increases and the water bound to pores starts to melt. The bound water continues to melt until around 273 K (0^oC) there is a very sharp increase in signal and this is where the bulk water melts. The final height of the line represents the total amount of water in the sample. One of the samples had bone attached than others (red line) and it has the highest signal because it contains noticeable more water than other samples. Other lines appear to be in quite same position and the double freezing do not appear to affect one of the samples (blue line).

On Figure 16, there is again the amount of melted water as a function of time from the human cartilage spin echo data. From that, the derivative of the slope is converted to a pore size distribution using a modified Gibbs-Thomson equation. If assumed that the k value of the Equation 17 is $10 \cdot 10^{-8}$ Km and the pores are cylindrical in shape, all samples show a single peak at about 1.5 nm diameter. This result seems to be quite comparable because, for example, in an article *Cartilage and diarthrodial joints as paradigms for hierarchical materials and structures (Mow, Biomaterials)* [16] shows that the distance between closely spaced negatively charged proteoglygan molecules is 1-1.5 nm. For this reason, it can be assumed that water might be bound to proteoglycans at low temperatures. In addition, the sample with bone attached (yellow line), shows a lower peak at about 8 nm but it cannot be said for sure if this is some actual pore size or just an error.

Figure 17 represents the effect of change of collagen and chondroitin sulfate in the protein gels. On left, the amount of chondroitin sulfate is kept constant and different lines represent the varying amounts of collagen, and on the contrary on right, the amount of collagen is kept constant and the amount of chondroitin sulfate changes. On both graphs representing the signal as a function of temperature, it can be seen that lines representing different samples seems to be on different heights but it cannot be said for sure if the collagen and CS have a clear effect on the amount of bound water because the used gel samples did not have exactly same volume. The corresponding pore size distribution graphs are quite noisy but in both graphs there

can be seen two separate peaks around 10 nm. The pore size of the gels is larger than in cartilage samples because the composition of the gels is very simplified and it is impossible to make an artificial sample as dense as the real extracellular matrix is.

On Figure 18, there is represented the effect of varying CS and collagen concentrations on T_2 relaxation times on protein gels. It can be seen that if the temperature rises or the concentration of collagen decreases, the T_2 relaxation time of bound water increases. Opposite, the amount of CS does not seem to affect to T_2 but rise of temperature does. One of the samples (Collagen=40, CS=5) differs slightly from others but because other lines are aligned, it can be said that the amount of CS does not affect the T_2 of protein gels.

To summarize, these experiments show clearly that there is bound water in articular cartilage. Graphs showing amount of signal as a function of temperature follow the Gibbs-Thomson equation as expected and a clear depression in melting point can be seen. Based on this study, the pore size of human articular cartilage is approximately 1.5 nm which is a reasonable result. The amount of collagen in gel samples seems to have an effect on T_2 relaxation times but the amount of chondroitin sulfate does not.

These results give useful information about bound water and porous structure in articular cartilage and because these experiments worked well, this study will be continued to get even more accurate and detailed data. The function of articular cartilage depends essentially on the water components it contains and knowledge about bound water can help resolve many aspects of cartilage function. All in all, comprehensive research on articular cartilage is important to understand better cartilage function and to develop prevention and new therapies to join diseases such as osteoarthritis affecting millions of people worldwide.

References

[1] Gordon Betts J, Desaix P, Johnson E, Johnson JE, Korol O, Kruse D, et al. Anatomy and Physiology. Rice University. OpenStax; 2013.

[2] Goldring MR. Articular Cartilage Degradation in Osteoarthritis. HSS J. 2012; 8(1): 7–9.

[3] Telkki V. 761359A Spectroscopic methods, NMR spectroscopy. University of Oulu. Lecture material 2018. In Finnish.

[4] Keeler J. Understanding NMR Spectroscopy. Second Edition. John Wiley & Sons; 2010.

[5] Chen X, Weber I, Harrison RW. Hydration water and bulk water in proteins have distinct properties in radial distributions calculated from 105 atomic resolution crystal structures. Journal of Physical Chemistry B. 2008; 112(38): 12073-12080.

[6] Wehrli FW, Fernández-Seara MA. Nuclear magnetic resonance studies of bone water. Annals of Biomedical Engineering. 2005; 33(1): 79-86.

[7] Figure 2. Brody LT. Knee osteoarthritis: Clinical connections to articular cartilage structure and function. Physical Therapy in Sport. 2015; 16(4): 301-16.

[8] Figure 3. Oussorena E, Brands MMMG, Ruijter GJG, van der Ploeg AT, Reuser AJJ. Bone, joint and tooth development in mucopolysaccharidoses: Relevance to therapeutic options. Biochimica et Biophysica Acta (BBA) - Molecular Basis of Disease. 2011; 1812(11): 1542-1556.

[9] Fox AJS, Bedi A, Rodeo SA: The Basic Science of Articular Cartilage: Structure, Composition and Function. Sports Health. 2009; 1(6): 461–468.

[10] Stockwell RA. Chondrocytes. J Clin Pathol Suppl (R Coll Pathol). 1978; 12: 7–13.

[11] Bhosale A, Richardson J. Articular cartilage: structure, injuries and review of management. British Medical Bulletin. 2008; 87(1): 77-95.

[12] Suomen Nivelyhdistys ry. In Finnish. [Cited 1.8.2019].
`http://www.nivel.fi/tietoa-nivelista/nivelrikko.html`

[13] Pearle AD, Warren RF, Rodeo SA. Basic Science of Articular Cartilage and Osteoarthritis. Clin Sports Med. 2005; 24: 1–12.

[14] Buckwalter JA, Mankin HJ, Grodzinsky AJ. Articular cartilage and osteoarthritis. AAOS Instructional Course Lectures. 2005; 54: 465-80.

[15] Neogi T. The Epidemiology and Impact of Pain in Osteoarthritis. Osteoarthritis Cartilage. 2013; 21(9): 1145–1153.

[16] Ghiassi-Nejad M, Torzilli PA, Peemoeller H, Pintar MM. Proton spin-spin relaxation study of molecular dynamics and proteoglycan hydration in articular cartilage. Biomaterials. 2000; 21: 2089-2095.

[17] Mow VC, Ratcliffe A, Poole AR. Cartilage and diarthrodial joints as paradigms for hierarchical materials and structures. Biomaterials. 1992; 13(2): 67-97.

[18] Hornak JP. The Basics of NMR. 1997-2017. [Cited 1.8.2019].
http://www.cis.rit.edu/htbooks/nmr/

[19] Figure 4. Process NMR. [Cited 1.8.2019].
https://www.process-nmr.com/principles-of-nmr/

[20] Seppänen R, Mannila L, Kervinen M, Parkkila I, Konttinen P et al. MAOL table book. Otava; 2013.

[21] Figure 5. Wikimedia Commons. [Cited 2.10.2019].
https://commons.wikimedia.org/wiki/File:T1_relaxation.jpg
https://commons.wikimedia.org/wiki/File:T2_relaxation.jpg

[22] Figure 6. Wikimedia Commons. [Cited 1.8.2019].
https://commons.wikimedia.org/wiki/File:Nmr_fid_good_shim_EN.svg

[23] Figure 7. Chemistry LibreTexts. [Cited 26.8.2019]
https://chem.libretexts.org/Bookshelves/Physical_and_Theoretical_Chemistry_Textbook_Maps/Supplemental_Modules_(Physical_and_Theoretical_Chemistry)/Spectroscopy/Magnetic_Resonance_Spectroscopies/Nuclear_Magnetic_Resonance/NMR%3A_Theory/Relaxation

[24] Figure 8. Wikimedia Commons. [Cited 26.8.2019]
https://commons.wikimedia.org/wiki/File:Spin_Echo_Diagram.png

[25] Figure 9. Chemistry LibreTexts. [Cited 2.10.2019]
https://chem.libretexts.org/Bookshelves/Physical_and_Theoretical_Chemistry_Textbook_Maps/Supplemental_Modules_(Physical_and_Theoretical_Chemistry)/Spectroscopy/Magnetic_Resonance_Spectroscopies/Nuclear_Magnetic_Resonance/NMR%3A_Experimental/Pulse_Sequences

[26] Claridge TDW. High-Resolution NMR Techniques in Organic Chemistry. Elsevier; 2016.

[27] Figure 11. Wikimedia Commons. [Cited 1.8.2019]
https://commons.wikimedia.org/wiki/File:Fourier_transform_time_and_frequency_domains_(small).gif

[28] Petrov OV, Furo I. NMR cryoporometry: Principles, applications and potential. Progress in Nuclear Magnetic Resonance Spectroscopy. 2009; 54: 97–122.

[29] Mitchell J, Webber JBW, Strange JH. Nuclear magnetic resonance cryoporometry. Physics Reports 461. 2008; 461: 1–36.